CrossMark

ORIGINAL ARTICLE

On time–temperature-dependent viscoelastic behavior of an amorphous polyimide

Thibaut Crochon[1] · Chun Li[2] · Martin Lévesque[1]

Abstract Development of new polyimide formulas has led to an increase of the use of polymer matrix composites by the aerospace industry in critical applications such as aircraft engines. In such an extreme environment, the polymer matrix is likely to exhibit a viscoelastic behavior due to the elevated temperatures. Furthermore, physical ageing is likely to appear during the service life of the material. In order for engineers to design with such materials, constitutive theories able to take into account those effects, must be developed. This paper deals with the mechanical behavior of a new polyimide matrix tested under complex thermo-mechanical histories while accounting for physical ageing. The experimental data obtained was modeled with a newly developed constitutive theory stemming from Schapery's thermodynamical framework. The model parameters were obtained from creep-recovery data under various temperatures, ageing times, and loads. The model was subsequently validated against independent complex thermo-mechanical histories. An excellent agreement between the experiments and the predictions has been obtained.

Keywords Viscoelasticity · Physical ageing · Temperature · Modeling

1 Introduction

Firstly used in nonstructural applications, polymer matrix composites (PMCs) are now widely used in more critical aerospace applications, such as wings, fuselage, and aircraft engines. Aircraft engine applications require materials able to withstand extreme service conditions, such as elevated temperatures, high mechanical loadings, and a highly oxidative environment. With rated service temperatures exceeding 300 °C, overall excellent me-

✉ M. Lévesque
  martin.levesque@polymtl.ca

[1] CREPEC, Département de Génie Mécanique, École Polytechnique de Montréal, C.P. 6079, succ. Centre-ville, Montréal, Québec, H3C 3A7, Canada

[2] Aerospace, National Research Council, 1200 Montreal Road, Building M-3, Ottawa, K1A 0R6, Canada

chanical properties and the possibility to be manufactured through easier and cheaper out-of-autoclave processes such as resin transfer molding (RTM), polyimide-based PMCs set themselves as potential candidates for such applications (Li et al. 1999).

Polymer matrices exposed to high temperatures and loads are likely to exhibit a viscoelastic behavior, potentially nonlinear with respect to load and temperature. In addition, the combined effects of elevated temperature and the environment near the engines are likely to increase physical and chemical ageing (Xiao et al. 1994). For example, Marais and Villoutreix (1998) realized a series of creep and recovery tests on PMR-15 polyimide matrix and found that the material compliance significantly increased with increasing stress and temperature levels. Furthermore, at temperatures far below the glass transition temperature (T_g), the material seemed to exhibit a linearly viscoelastic behavior. However, as the test temperatures increased, the same stress levels led to a nonlinearly viscoelastic behavior. Therefore, adequate constitutive theories must take in account these nonlinear effects, and representative experimental data have to be used to obtain meaningful material properties.

For many years, PMR-15 was the preferred polyimide for structural applications since it offered stable performances at high temperatures, while being easy and relatively cheap to process (Jones 2009). However, its use has decreased in recent years since one of its core components was found to be carcinogenic. Alternatives to PMR-15 were subsequently developed, like the MVK-10 polyimide developed my Maverick Corporation.

The purpose of this work was to study the mechanical behavior of the MVK-10 polyimide submitted to a wide range of elevated temperatures. The dependence of the material viscoelasticity on temperature and physical ageing was examined, and a model based on Schapery's framework (Schapery 1964) was developed and validated against independent complex thermo-mechanical histories.

This paper is organized as follows. Section 2 recalls the notions of physical ageing and shift factors. Section 3 presents the procedure used to test the material. Finally, Sect. 4 deals with the development of the model and the determination of its parameters from the experiments.

Stresses/strains and stiffnesses/compliances are respectively represented as vectors and matrices, according to the modified Voigt notation recalled in Lévesque et al. (2008). Vectors are denoted by boldfaced lower case letters, for example, $\boldsymbol{a}$ and $\boldsymbol{\alpha}$, and matrices are denoted by boldfaced capital Roman letters, for example, $\mathbf{A}$.

2 Background

2.1 Physical ageing

Firstly developed for the case of polymers submitted to elevated temperatures (Williams et al. 1955), the time-superposition principle (TSP) has been extended to physical ageing by Struik (1978). Based on the free-volume theory, the TSP relies on the effective time concept (Bradshaw and Brinson 1997b) to compare creep responses obtained at different temperatures and ageing times. The concept implies that retardation times under any service conditions can be related to those at reference conditions by a simple multiplicative horizontal shift factor. The concept is mainly used for predicting polymers' long-term creep (Ohashi et al. 2002; Olasz and Gudmundson 2005; Zhao 2008; Luo 2007) or physical ageing responses at a given temperature by testing the material at higher temperatures over shorter time scales.

According to the TSP, the creep compliance $S(t)$ of a material aged for a time t_e at a constant temperature T and submitted to a stress σ can be related to its creep compliance $\bar{S}(t)$ when aged for a reference time $\bar{t}_e$ at a reference temperature $\bar{T}$ and submitted to a reference stress $\bar{\sigma}$, according to

$$S(t) = b(t_e, T, \sigma)\bar{S}\left(\frac{t}{a(t_e, T, \sigma)}\right), \tag{1}$$

where $a(t_e, T, \sigma)$ and $b(t_e, T, \sigma)$ are respectively horizontal and vertical shift factors dependent on temperature, stress, and physical ageing. Graphically, those shift factors represent the distance by which $S(t)$ must be respectively shifted horizontally and vertically in order to match the reference master curve $\bar{S}(t)$ (Bradshaw and Brinson 1997b). The shift factor $a(t_e, T, \sigma)$ can be decomposed into the product of three shift factors, namely the temperature shift factor a_T, the stress shift factor a_σ, and the physical ageing shift factor a_{t_e} (Lai and Bakker 1996), leading to

$$a(t_e, T, \sigma) = a_T a_\sigma a_{t_e}. \tag{2}$$

The evaluation of the horizontal shift factor a_{t_e} is usually performed following the methodology proposed by Struik (1978), who considered the case where a material was quenched from a temperature above its glass transition temperature to a temperature T below its glass transition temperature. In this simple case, the ageing time t_e is defined as the time elapsed since the quench. Struik (1978) found that the shift factor a_{t_e} extracted from a creep test could be approximated by

$$a_{t_e} = \left(\frac{t_e}{\bar{t}_e}\right)^{\mu(T)}, \tag{3}$$

where $\mu(T)$ is the shift rate. In the case of isothermal ageing, the shift rate is assumed to remain constant as long as the material continues to age.

The simple relationship of Eq. (3) is not valid for general nonisothermal ageing histories due to memory effects (Bradshaw and Brinson 1997b). Two approaches dealing with general ageing histories distinguish themselves in the literature: (i) The continuous shift factor (CSF) method proposed by Bradshaw and Brinson (1997b) based upon the notion of effective ageing time; (ii) the KAHR-a_{t_e} method proposed by Guo et al. (2009), in which the ageing time is defined using volume relaxation theories. The CSF method is an adaptation of Eq. (3) to the case of nonisothermal ageing where t_e is replaced by the so-called effective ageing time t_e^{eff} defined as the time the material would have to age under isothermal conditions to achieve the same amount of physical ageing under nonisothermal conditions. The KAHR-a_{t_e} method relies on the KAHR theory for materials volume relaxation outside thermodynamic equilibrium (Kovacs 1963; Kovacs et al. 1979). In this theory, the amount of physical ageing is linked to the notion of relative depart from volumetric equilibrium δ (defined as the difference between the actual and equilibrium volumes of a material) by assuming that physical ageing can be related to δ by a simple linear relationship (Struik 1988; Guo et al. 2009).

Finally, whereas the introduction of a complementary vertical shifting $b(t_e)$ is often required when dealing with physical ageing, it is generally found to have a much smaller effect than the horizontal shift factor (Sullivan et al. 1993) and to exhibit an irregular behavior (Bradshaw and Brinson 1999). Consequently, a vertical shift in the case of physical ageing is considered to be negligible and is not included into the final model. Nevertheless, some authors found that, in some cases, a general trend could be observed in which the vertical shift factor decreases with increasing ageing times (Sullivan et al. 1993;

Bradshaw and Brinson 1997a). This decrease of the vertical shift factor with increasing age-ing times is consistent with the general increase in stiffness observed in physically aged polymers. Bradshaw and Brinson (1997a) even proposed that a linear relationship could be observed when representing the vertical shift factor as a function of the logarithm of ageing time. However, in the general case of TSP, the vertical shift factor is assumed to be only temperature-dependent.

2.2 Schapery's constitutive theories

The TSP is useful for evaluating the linearly viscoelastic properties of a material in reference conditions over a wide range of decades with limited experimental data. However, dealing with nonlinear behavior under challenging environmental conditions requires more general models. Many nonlinear models have been developed by enforcing that the mathematical operator relating strains and stresses meets the principles of thermodynamics, irrespectively of the loading histories (Lévesque et al. 2008). Such a strategy was developed by Biot (1954) in the case of linearly viscoelastic materials within the framework of the thermodynamics of irreversible processes. It was then extended to nonlinearly viscoelastic materials by Schapery (1964) by the introduction of nonlinearizing functions. Such phenomenological theories can be seen as extensions of the TSP to complex loading and temperature histories. The horizontal shift factor is replaced by the so-called material clock, which has been developed for a variety parameters including free volume (Knauss and Emri 1981; Knauss and Emri 1987), strains (Schapery 1966a), stresses (Schapery 1966b), physical age-ing (Schapery 1997), or any their combination (Lai and Bakker 1996). More complex material clocks were also developed to take into account the general state of the material by using quantities such as the entropy (Drozdov 1997) or the internal energy (Caruthers et al. 2004).

Schapery's (Schapery 1964) framework has been extended and interpreted in a number of papers over the last forty years and led to a three-dimensional stress-based hereditary integral:

$$\boldsymbol{\varepsilon}(t) = \frac{\partial \varphi}{\partial \boldsymbol{\sigma}} + \mathbf{G}_1(t) : \int_0^t \Delta \mathbf{S}(\Omega - \Omega') : \frac{\mathrm{d}}{\mathrm{d}\tau}\big[g_2(\tau)\boldsymbol{\sigma}(\tau)\big]\,\mathrm{d}\tau, \qquad (4)$$

where $\boldsymbol{\varepsilon}$ is the mechanical strain tensor, φ is a stress potential, and $\Delta \mathbf{S}$ is the transient compliance tensor. The potential φ can be defined as follows (Schapery 1997; Lévesque et al. 2008):

$$\frac{\partial \varphi}{\partial \boldsymbol{\sigma}} = g_0(t)\mathbf{S}_0 : \boldsymbol{\sigma}(t), \qquad (5)$$

where $\mathbf{S}_0$ is an instantaneous creep compliance. The tensor $\Delta \mathbf{S}$ can be expressed as a Kohlrausch's stretched exponential function (Guo and Bradshaw 2007; Guo and Bradshaw 2009; Guo et al. 2009), a Prony series (Lai and Bakker 1996; Haj-Ali and Muliana 2004), or a power-law function (Ruggles-Wrenn and Broeckert 2009). Using a Prony series leads to

$$\Delta \mathbf{S}(t) = \sum_{n=1}^{N} \mathbf{S}_n\big(1 - \exp[-\lambda_n t]\big), \qquad (6)$$

where $\mathbf{S}_n$ are the transient compliance coefficients associated to the inverted retardation times λ_n. Schapery (1964) introduced the notion of reduced time Ω, which is a generaliza-

tion of the horizontal shift factors introduced in Eq. (2), as

$$\Omega(t_e, T, \sigma) = \int_0^t \frac{\mathrm{d}\xi}{a_T(\xi) a_\sigma(\xi) a_{t_e}(\xi)}. \tag{7}$$

Finally, g_0, $\mathbf{G}_1$, and g_2 are the nonlinearizing functions introduced to represent the nonlinearly viscoelastic behavior. Those functions could be considered as a generalization of the vertical shift factors $b(t_e, T, \sigma)$.

It should be noted that development of the three-dimensional theory in Eq. (4) leads to

$$\mathbf{G}_1(t) = \gamma(t)\mathbf{I} + \frac{\mathrm{d}\gamma(t)}{\mathrm{d}\boldsymbol{\sigma}} \otimes \boldsymbol{\sigma}, \tag{8}$$

where $\mathbf{I}$ is the fourth-order identity tensor, and γ is a function of the stress tensor. Therefore, $\mathbf{G}_1$ is a fourth-order tensor in the general case. It can be reduced to a scalar and the identity tensor for a very limited number of situations (see Lévesque et al. 2008 for more details).

Development of models for the nonlinearizing functions have mainly focused on stresses or strains nonlinearizing effects (Lai and Bakker 1996; Haj-Ali and Muliana 2004; Lévesque et al. 2008). For example, Schapery (1997) considered the nonlinearizing functions to be quadratic functions of stresses. Lai and Bakker (1996) proposed that function g_0 be dependent of the first stress invariant, whereas $\mathbf{G}_1$ and g_2 would be dependent on the effective octahedral shear stress. Haj-Ali and Muliana (2004) proposed that all nonlinearizing functions be polynomial functions of the effective octahedral shear stress. Sawant and Muliana (2008) proposed temperature-dependent nonlinearizing functions by assuming that g_0 was a linear function, whereas $\mathbf{G}_1$ and g_2 were exponential functions of the temperature, and Muliana and Sawant (2009) assumed that all three functions were polynomial functions of temperature. However, to the knowledge of the authors, a model for the nonlinearizing functions depending on physical ageing has yet to be proposed.

3 Experimental method and data

Note that the experimental data related to the MVK-10 resin is proprietary to the industrial sponsors. For this reason, we have:

- The stress values normalized with respect to σ_{max}, which is the ultimate tensile strength obtained from the tensile tests at wet-$T_g - 28$ °C on nonaged samples (see further for the wet-T_g definition);
- The temperatures expressed with respect to the wet-T_g;
- The creep compliances normalized with respect to $\bar{S}_0$, which is the instantaneous creep compliance at wet-$T_g + 37$ °C and for an ageing time $\bar{t}_e$ of 32 hours;
- The strains normalized with respect to ε_f, which is the strain at failure obtained from tensile tests on nonaged samples at wet-$T_g - 28$ °C;
- The displacements normalized with respect to the maximum displacement δ_0 measured during the three-point bending creep–recovery tests performed at wet-$T_g + 37$ °C and for a creep stress $\sigma_0 = 0.5\sigma_{\mathrm{max}}$.

3.1 Material

The material studied was the MVK-10 polyimide from Maverick Corporation. Panels were prepared using RTM and cured at a temperature slightly above MVK-10's T_g for approx-

Fig. 1 Samples water saturation conditioning prior to the wet-T_g measurements. The samples were assumed to be fully water saturated when their masses stabilized after a prolonged period of conditioning. The *error bars* represent 95 % confidence intervals on the mean value computed from three samples
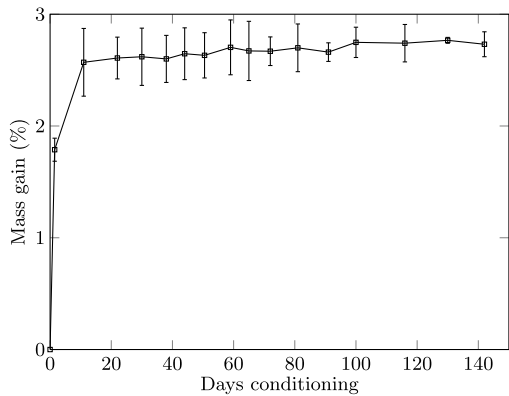
imately 4 hours before being subsequently post-cured at the same temperature for other 17 hours; three panels of 381 mm × 317.5 mm × 5.2 mm and one panel of 381 mm × 317.5 mm × 12.7 mm were available for this project.

The material's dry- and wet-glass transition temperatures, dry-T_g and wet-T_g, were investigated with a dynamic mechanical analyzer (DMA) TA Q800 from TA Instruments and according to ASTM D7028 standard. Samples of 60 mm × 6.75 mm × 5.2 mm were obtained by water jet cutting from the flat panels. Prior to testing, dry-T_g samples were left to dry for 48 hours in an oven at a temperature of 50 °C before being cooled down and stored in a desiccator. Wet-T_g samples were fully saturated with water in an environmental chamber. Their masses were recorded regularly until no more gains were observed. Figure 1 reports the samples mass gain as a function of the number of days of conditioning. It can be seen that the saturation occurred very quickly. The samples were subsequently loaded at a frequency of 1 Hz under strain control while being heated at a constant rate of 5 °C·min^{-1}. As is customary of aerospace applications, the T_g was determined as the intersection of the two slopes associated to the storage modulus E' for the glassy and rubbery states.

The wet-T_g was found to be more than 60 °C lower than the dry-T_g. As per Federal Aviation Administration regulations, the service temperature of the polyimide was defined as wet-$T_g - 28$ °C. Whereas the actual value of the wet-T_g cannot be revealed for confidentiality reasons, it was well in excess of 200 °C.

It should be noted that the wet-T_g tests lasted for less than 1 hour. Since the samples were relatively thick and conditioned for an extended period of time, the effect of water evaporation on the wet-T_g measurement was assumed to be negligible.

3.2 Mechanical testing

Tensile and three-point bending testing was conducted with an MTS Insight 50-kN electromechanical load frame equipped with a Lab-Temp LBO-series box environmental chamber from Thermcraft Incorporated. The environmental chamber allows for testing at temperatures up to 425 °C with a maximum heating rate of 10 °C·min^{-1}. The chamber's temperature was manually set so as to ensure that a thermocouple directly attached to the specimen's gage section (tensile tests) or very close to it (bending tests) recorded the target temperature.

Note that mechanical testing was carried out on dry samples. Fully water saturated samples were only used for the wet-T_g determination.
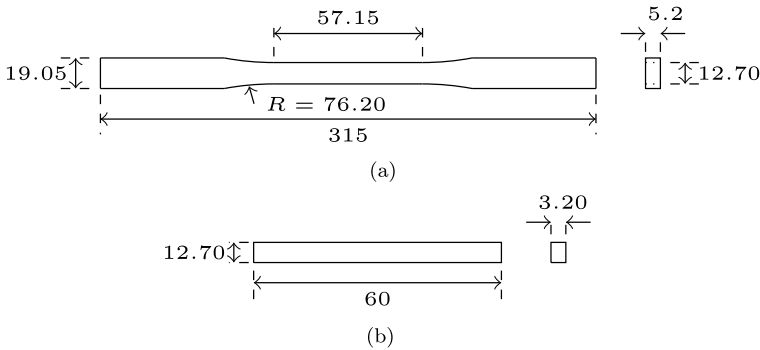
Fig. 2 Dimensions in mm of the samples used: (**a**) ASTM Type I specimen for tensile testing, (**b**) ASTM D638 specimen for three-point bending testing

3.2.1 Tensile testing

Tensile tests were performed on nonaged samples at wet-$T_g - 28$ °C according to ASTM D638 standard, and coupons were designed in compliance with ASTM D638 and ASTM D2990 standards for tensile and tensile creep testing of plastics, respectively. Some dimensions had to be adjusted to allow for proper gripping (see Fig. 2a).

Strains were measured with Vishay WK-06-125TM-350 tee rosettes to measure axial and transverse strains. These rosettes were bonded with Vishay M-Bond 610 Adhesive on both sides of the samples to account for specimen bending or initial curvature.

Three tensile tests at wet-$T_g - 28$ °C were performed to evaluate the tensile stress up to failure (σ_{max}). The tests were conducted under displacement control at a rate of 5 mm·min^{-1}. The resulting standard deviation was less than 5 % of σ_{max} mean value. Creep tests at wet-$T_g - 28$ °C were also performed under different stress levels to assess the material's linearity. The axial creep compliance $S(t)$ and Poisson's ratio $\nu(t)$ were computed as

$$S(t) = \frac{\varepsilon_l(t)}{\sigma_0}, \tag{9a}$$

$$\nu(t) = -\frac{\varepsilon_t(t)}{\varepsilon_l(t)}, \tag{9b}$$

where σ_0 is the creep stress, and $\varepsilon_l(t)$ and $\varepsilon_t(t)$ are the axial and transverse strains, respectively. Figures 3 and 4 plot the normalized creep compliances and Poisson's ratio computed for different values of σ_0. The results show that the stress level had a negligible impact on the creep compliance and the viscoelastic Poisson's ratio at wet-$T_g - 28$ °C. Tensile tests could not be performed at higher temperatures since strain gages were not rated for such temperatures. Therefore, the effect of stress on the creep compliance was further investigated with three-point bending tests. The viscoelastic Poisson's ratio was considered to be stress-independent for all temperatures.

3.2.2 Three-point bending testing

Owing to their costs, only a limited number of MVK-10 panels were available. Three-point bending testing was used to study the effect of ageing since it required much smaller samples than tensile testing. The tests were performed at temperatures ranging from wet-$T_g - 28$ °C to wet-$T_g + 37$ °C. A homemade fixture was designed in compliance with ASTM D790

Fig. 3 Impact of stress level on the creep compliance at wet-$T_g - 28$ °C for nonaged samples, normalized by $\bar{S}_0$
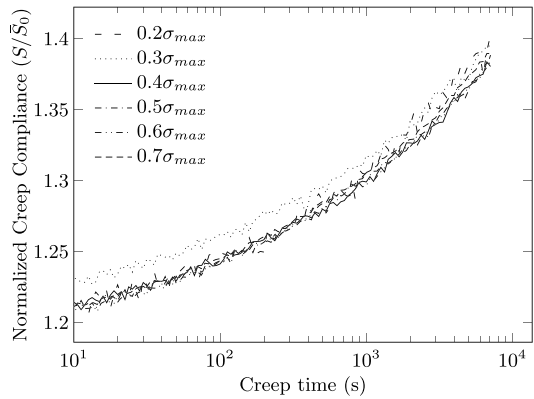
Fig. 4 Impact of stress level on the Poisson's ratio at wet-$T_g - 28$ °C for nonaged samples, normalized by that obtained for a creep stress of $0.5\sigma_{\max}$ and evaluated at $t = 0$ (referred to as ν_0)
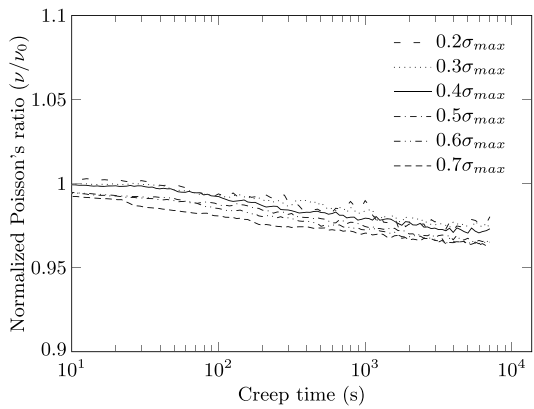
and ASTM D2990 standards. The loading nose and supports had cylindrical surfaces with radii of 5.0 mm. The span between the two supports was of 50 mm. The loading nose was attached to a 1-kN loadcell whose crosshead was controlled by MTS TestWorks 4 software. The load cell allowed for measuring loads at ± 0.1 N, and the crosshead's displacement was evaluated with an accuracy of 0.01 mm. Rectangular samples, designed in compliance with ASTM D2990 standard (Fig. 2b), were cut with a high-precision low-speed saw equipped with a diamond wafering blade.

The maximum deflection δ at the middle of the sample was directly obtained from the crosshead's displacement. The flexural stress σ and strain ε were computed according to the well-known formulas

$$\sigma = \frac{3PL}{2wd^2}, \tag{10a}$$

$$\varepsilon = \frac{6d\delta}{L^2}, \tag{10b}$$

where P is the applied load, L is the span between the supports, and w and d are respectively the sample's width and thickness.

Series of creep tests were performed at various temperatures using the methodology proposed by Struik (1978) for short-term isothermal ageing tests to investigate the dependence of the polymer's mechanical properties to temperature, stress, and physical ageing. The material was first heated to the testing temperature, and then a series of creep and recovery
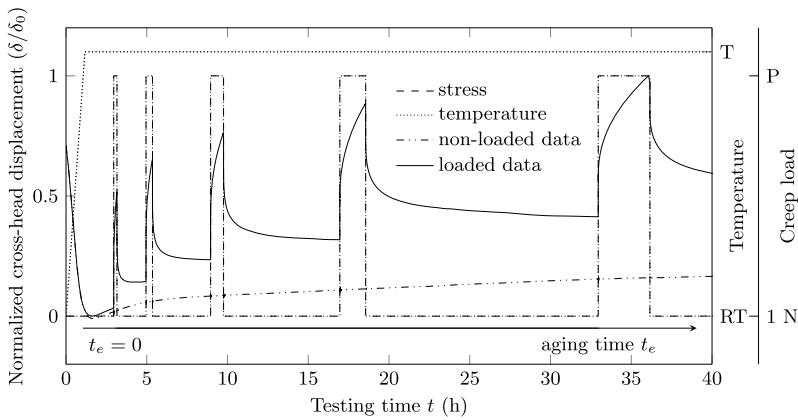
Fig. 5 Typical temperature and loading histories applied to the three-point bending samples. The displacements were normalized by the maximum displacement measured at wet-T_g + 37 °C and for a creep stress $\sigma_0 = 0.5\sigma_{max}$. "RT" stands for room temperature, "T" stands for the testing temperature, and "P" is the applied load inducing the creep stress σ_0. The material was first heated at the ageing temperature, and then a series of creep and recovery tests was performed at increasing time intervals. The first creep test began two hours ($t_e = 2$ h) after the ageing temperature was reached. Subsequent creep and recovery tests began at $t_e = 4$ h, $t_e = 8$ h, $t_e = 16$ h, and $t_e = 32$ h. Nonloaded data, that is, crosshead's displacement for a constant load of 1 N, are used as baseline. Physical ageing was assumed to start when the testing temperature was reached inside the environmental chamber (it is denoted by $t_e = 0$ on the graph)

tests were performed at increasing time intervals, with the duration of each creep test equal to 10 % of the total ageing time (for physical ageing considered as constant during a creep test). It should be noted that Struik recommends to initiate each test by a so-called rejuvenation period in which the material is heated slightly above its glass transition temperature for a few minutes to erase all previous ageing histories. However, such rejuvenation periods led to a severe thermal degradation for the material investigated in this study. Therefore, for all tests, samples were directly heated to the test temperature without any rejuvenation period. All the three-point bending samples were cut from the same panel and thus had the same ageing history. Furthermore, the ageing history prior to testing was assumed to have a negligible effect on mechanical properties since the panels were stored at room temperature, which is much lower than wet-T_g − 28 °C.

Physical ageing was investigated at five temperatures, namely, wet-T_g − 28 °C, wet-T_g − 3 °C, wet-T_g + 7 °C, wet-T_g + 22 °C, and wet-T_g + 37 °C. For each temperature, the tests were repeated at three stress levels, namely, $0.1\sigma_{max}$, $0.25\sigma_{max}$, and $0.5\sigma_{max}$, where σ_{max} is the ultimate stress at wet-T_g − 28 °C (obtained from the tensile tests). Each test was performed once.

The three-point bending setup and sample intrinsic thermal expansions were measured to isolate the deflection only associated to mechanical loading. Correction tests were performed at each testing temperature by submitting a sample to a small contact load of 1 N. Data from one such correction test can be found in Fig. 5. The figure shows that the initial increase in temperature is accompanied by an overall thermal expansion of the setup (which is represented by a negative crosshead's displacement). Once the test temperature was achieved, the crosshead's displacement reached a minimum before starting to increase. This increase in the crosshead's displacement can be explained by three phenomena: (i) a creep behavior induced by the contact load of 1 N, (ii) a contraction of the polymer sample due to physical
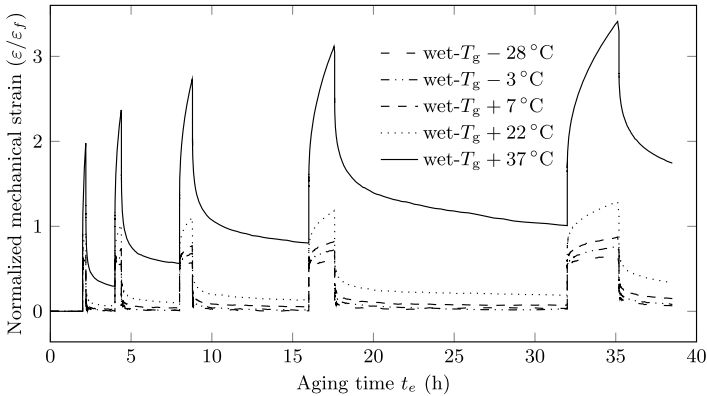
Fig. 6 Corrected creep and recovery data, that is, thermal strains have been removed using the correction data, for the five testing temperatures for a creep stress of $0.5\sigma_{max}$. The mechanical strain was normalized by ε_f. The first creep test began two hours ($t_e = 2\,\text{h}$) after the ageing temperature was reached. Subsequent creep and recovery tests began at $t_e = 4\,\text{h}$, $t_e = 8\,\text{h}$, $t_e = 16\,\text{h}$, and $t_e = 32\,\text{h}$

ageing as the polymer evolves towards its thermodynamic equilibrium, and (iii) a thermal expansion creep.

The correction data was subtracted from the creep and recovery data to obtain the samples deflections due to mechanical loading, leading to displacement data like that reported in Fig. 6. It should be noted that this correction removes the crosshead's displacement due to the three phenomena explained before. In particular, it removed the volume contraction due to physical ageing. However, it does not remove the impact of physical ageing on the material's mechanical properties. This was possible since the material exhibited a linearly viscoelastic behavior in the testing range. It can be seen that increasing the test temperature leads to a much more compliant material. It can also be seen that the material does not fully recover between two creep tests for higher test temperatures. Since the creep compliances are independent of the stress level, even at the higher temperatures, this phenomenon is due to neither plasticity nor viscoplasticity. It can however be explained by the general increase in the material's stiffness due to physical ageing. For example, assume a viscoelastic material with one inverted retardation time λ_1 aged at constant temperature and with an ageing shift rate $\mu = 1$. The material is submitted to a creep–recovery test. The creep duration is t_1. Then, it can be shown that the recovery strain is

$$\boldsymbol{\varepsilon}(t > t_1) = \bar{\mathbf{S}}_1 : \boldsymbol{\sigma} \exp\big(-\lambda_1 \bar{t}_e [\ln t - \ln t_1]\big)\big[1 - \exp\big(-\lambda_1 \bar{t}_e [\ln t_1 - \ln 0]\big)\big]$$
$$\approx \bar{\mathbf{S}}_1 : \boldsymbol{\sigma} \exp\big(-\lambda_1 \bar{t}_e [\ln t - \ln t_1]\big). \tag{11}$$

Therefore, the smaller the quantity $\lambda_1 \bar{t}_e$ is, the longer the recovery strain requires to dissipate. As physical ageing increases, λ decreases, which explains why at higher temperatures, the material needs longer times to recover and residual strains build-up.

Figure 7 shows the strain-to-stress ratio curves during the creep phase for the material for an ageing time of 32 h at wet-$T_g + 37$ °C and the three stress levels. Note that these curves are only an approximation of the compliance since the strains from the previous creep period were not fully recovered. This result is typical of what was obtained after various ageing times and at various temperatures and suggests that, in the range of stress and temperature used in the three-point bending tests, the material can be considered as linearly viscoelastic.

Fig. 7 Strain-to-stress ratio curves (normalized by $\bar{S}_0$) during creep for the material for an ageing time of 32 h at wet-$T_g + 37$ °C and three stress levels
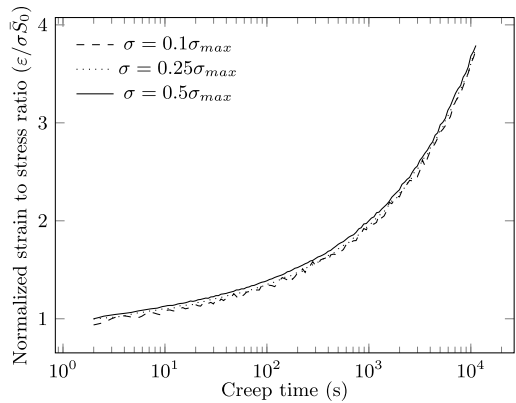
4 Results analysis

4.1 Model developments

The purpose of this section is to specialize Eq. (4) to the specific material and physical phenomena studied in this work.

Experimental data from tensile and three-point bending tests have shown that the material is linearly viscoelastic (with respect to stresses) and that its Poisson's ratio ν can be assumed as time-independent. Therefore, the three-dimensional compliance $\bar{\mathbf{S}}(t)$ can be reduced to

$$\bar{\mathbf{S}}(t) = \bar{S}(t) \begin{pmatrix} 1 & -\nu & -\nu & 0 & 0 & 0 \\ -\nu & 1 & -\nu & 0 & 0 & 0 \\ -\nu & -\nu & 1 & 0 & 0 & 0 \\ 0 & 0 & 0 & 1+\nu & 0 & 0 \\ 0 & 0 & 0 & 0 & 1+\nu & 0 \\ 0 & 0 & 0 & 0 & 0 & 1+\nu \end{pmatrix}. \tag{12}$$

Since the material is considered as linearly viscoelastic, $\frac{d\gamma(t)}{d\sigma} = 0$ in Eq. (8). Therefore, $\gamma(t)\mathbf{I}$ can be reduced to a scalar, and the fourth-order tensor $\mathbf{G}_1$ becomes the scalar g_1, and the three-dimensional constitutive theory of Eq. (4) can be reduced to a one-dimensional expression. Furthermore, Bradshaw and Brinson (1999) showed that, in the case of a linearly viscoelastic material submitted only to temperature and physical ageing, g_0 and g_1 could be set as equal, and g_2 could be set to unity. Previous studies (Sullivan et al. 1993; Bradshaw and Brinson 1999) have shown that g_0 could generally be considered as independent of physical ageing without any loss of accuracy. All those considerations led to the following model for the material studied:

$$\varepsilon(t) = g_0(T) \left[\bar{S}_0 \sigma(t) + \sum_{n=1}^{N} \bar{S}_n \int_0^t \left(1 - \exp\left[-\bar{\lambda}_n (\Omega - \Omega') \right] \right) \frac{d\sigma(\tau)}{d\tau} d\tau \right], \tag{13}$$

where

$$\Omega = \int_0^t \frac{dt'}{a_T a_{t_e}}. \tag{14}$$

The challenge lies in the determination of the temperature and physical ageing dependence of the nonlinearizing functions g_0, a_T, and a_{t_e}.

4.2 Optimization algorithm

The optimization made use of the three-point bending short-term isothermal ageing test data at different temperatures. The reference state was chosen as $\bar{T} = $ wet-$T_\mathrm{g} + 37\,°\mathrm{C}$ and $\bar{t}_e = 32\,\mathrm{h}$. The inverted relaxation times were fixed prior to the optimization with one time by decade on a logarithmic scale as

$$\bar{\lambda}_n \in \left\{ 10^{-6}\,\mathrm{s}^{-1}, \ldots, 10^1\,\mathrm{s}^{-1} \right\}. \tag{15}$$

The optimization of the material's properties was performed using the minimization algorithm `fmincon` from Matlab's optimization toolbox. The optimization problem solved by this function can be written as

$$\min_x \left(\sum_{i=1}^{I} \sum_{j=1}^{N_i} \left[F_{i,j} - \varepsilon_{i,j}(x) \right]^2 \right), \tag{16}$$

where $F_{i,j}$ and $\varepsilon_{i,j}$ are the experimental and predicted values for the jth data-point from the ith data-set, respectively, N_i is the number of data-points for the ith data-set, I is the number of data-sets (one for each temperature tested), and x is the set of material's parameters to be optimized.

4.2.1 Numerical implementation

The predicted values $\varepsilon_{i,j}(x)$ of the model presented in Eq. (13) were computed using the differential approach proposed by Crochon et al. (2010). This approach relies on the differential equations that are at the root of Schapery's hereditary integral and solves them with a backward-Euler finite-difference scheme. Adapted to Eq. (13), this approach leads to

$$\varepsilon_{i,j+1} = g_{0_{i,j+1}} \left[S_0 \sigma_{i,j+1} - A_2 \cdot \xi_{i,j+1} \right], \tag{17}$$

where ξ is the tensor of internal variables defined as

$$\xi_{i,j+1} = \left[I + \frac{\Delta t_{i,j}}{a_{T_{i,j+1}} a_{t_{e_{i,j+1}}}} A_3 \right]^{-1} \cdot \left[\xi_{i,j} - \frac{\Delta t_{i,j}}{a_{T_{i,j+1}} a_{t_{e_{i,j+1}}}} \sigma_{i,j+1} A_2 \right], \tag{18}$$

where A_2 is the $1 \times N$ matrix $[\sqrt{\lambda_1 S_1}, \ldots, \sqrt{\lambda_n S_n}, \ldots, \sqrt{\lambda_N S_N}]$, A_3 is the $N \times N$ matrix

$$A^{(3)} = \begin{bmatrix} \lambda_1 & & \\ & \ddots & \\ & \lambda_n & \\ & & \ddots & \\ & & & \lambda_N \end{bmatrix}, \tag{19}$$

and I is the $N \times N$ identity matrix, and $\Delta t_{i,j}$ is the time interval between the jth and $(j+1)$th data-points.

4.2.2 Extension to non-isothermal ageing

Nonisothermal ageing histories were accounted for by computing an equivalent ageing time, t_e^{equ}, used to obtain the ageing shift factor following the relationship

$$a_{t_{e_{i,j}}} = \left(\frac{t_{e_{i,j}}^{\mathrm{equ}}}{\bar{t}_e} \right)^{\mu_{i,j}}, \tag{20}$$

where t_e^{equ} represents the time the material needs to spend under isothermal conditions to achieve the same ageing shift factor a_{t_e} as in the complex thermal history. For example, if a material is aged for a time t_1 at a temperature T_1 before being aged for a time t_2 at a temperature T_2, then t_e^{equ} is the time the material would have to be isothermally aged at temperature T_2 to achieve the same ageing shift factor a_{t_e}. In this simple case, t_e^{equ} can be decomposed into two parts:

$$t_{e_{i,j}}^{equ} = t_{T_1 \to T_2} + t_{i,j} - t_1, \tag{21}$$

where $t_{T_1 \to T_2}$ is the time the material would have to spend at temperature T_2 to achieve the same amount of ageing as when aged at temperature T_1 for a time t_1. Since the ageing shift rate μ is considered as temperature-independent, $t_{T_1 \to T_2}$ can be easily computed according to

$$t_{T_1 \to T_2} = \frac{\mu(T_1)}{\mu(T_2)} t_1. \tag{22}$$

If a more complex thermal history was considered, for example the material was maintained at temperature T_0 for a time t_0 before being suddenly heated to temperature T_1 (the time to heat the material from T_0 to T_1 is considered negligible), then an equivalent time would have to be computed for t_1 in Eq. (22). Therefore, if a material is submitted to N consecutive thermal steps, its equivalent ageing time can be computed using the following relationship:

$$t_e^{equ} = t_{T_{N-1} \to T_N} + t_{i,j} - t_{N-1}, \tag{23}$$

where t_{N-1} is the time elapsed before the material was heated at the final temperature T_N ($t_{i,j} - t_{N-1}$ is the time elapsed since the last temperature jump), and $t_{T_{N-1} \to T_N}$ is defined following Eq. (22). This procedure was used in conjunction with Eq. (18) to predict the material's response under nonisothermal ageing histories.

4.2.3 Optimization results

A first optimization was performed in which the horizontal shift factor a_{t_e} was defined following the definition proposed in Eq. (3). In this case, the material's parameters to be optimized were the reference viscoelastic parameters $\bar{S}_0$, $\bar{S}_n$, and $\bar{\lambda}_n$ and the discrete values of $\mu(T)$, $a_T(T)$, and $g_0(T)$.

The results of this first optimization can be found in Figs. 8, 9, 10 and 11. An excellent agreement between predicted and experimental data was obtained for the creep and recovery phases and for all temperatures. Those results support the assumption of independence of g_0 on physical ageing. Analysis of the results shows that, in the range of temperature investigated, the shift rate linearly increases with temperature. Furthermore, the optimization led to $\mu = 0$ at the lowest temperature, meaning that no physical ageing is occurring that far from the glass transition temperature. Simultaneously, the shift factor a_T exhibits an exponential shape, whereas g_0 is constant for the lowest temperatures before abruptly increasing.

The second step of the optimization process aimed at determining the temperature-dependent functions for μ, a_T, and g_0. Based on the punctual values obtained in the first optimization run, the functions

$$\mu(T) = \mu_0 + \mu_1(T - \bar{T}), \tag{24a}$$

$$a_T(T) = \exp[a_0(\bar{T} - T)^{a_1}], \tag{24b}$$

$$g_0(T) = 1 + b_0 \operatorname{atan}[b_1(\bar{T} - T)], \tag{24c}$$
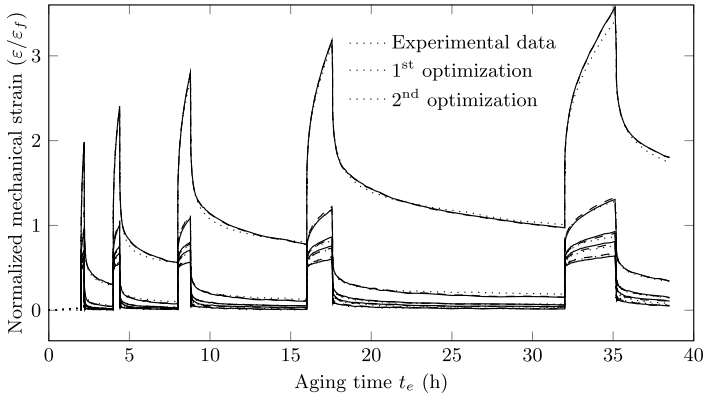
Fig. 8 Modeling of the material behavior using a Schapery-type constitutive theory with nonlinearizing functions depending on temperature and physical ageing. The curves correspond to the testing temperatures reported in Fig. 6. The strain was normalized by ε_f. The model shows an excellent fit with the experimental data for each temperature. The experimental data is represented with *dotted lines*, predictions of the first optimization with *dashed lines* and predictions of the second optimization with *solid lines*

Fig. 9 Evolution of the shift rate μ with respect to ageing temperature and physical ageing time. The first optimization values represent the results obtained without representing μ as a function, whereas the second optimization represents the results obtained for Eq. (24a)
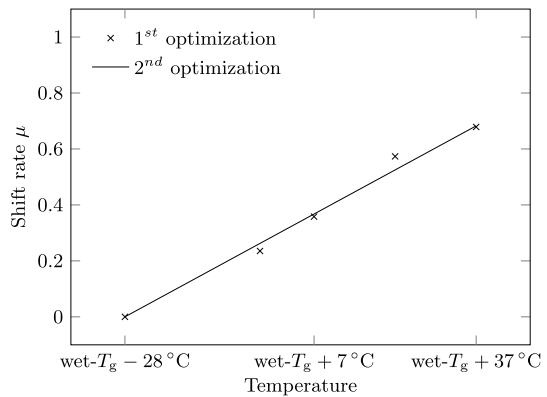

where μ_1, a_0, a_1, b_0, and b_1 are material parameters, were postulated, and their parameters were optimized with the same procedure as before. The parameter μ_0 was defined such as $\mu(\text{wet-}T_g + 37\,^\circ\text{C}) = 0$. The choice of the arctangent function to represent the temperature dependence of g_0 was motivated by the fact that it best represents the temperature-dependent behavior of polymers since it is bounded for arguments converging toward $\pm\infty$, that is, for temperatures far from the glass transition temperature, and also exhibiting a monotonic behavior.

The results of this second step in the optimization process can be found in Figs. 8 to 11, and the parameters are recapitulated in Tables 1 and 2. In overall, every function fits the results of the initial optimization.

4.3 Assessment of the ageing effect on the creep compliance

The mechanical testing performed in this work does not allow for directly obtaining the creep compliances from different ageing times since the strains from previous creep periods

Fig. 10 Evolution of the temperature-dependent horizontal shift factor a_T. The first optimization values represent the results obtained without representing a_T as a function, whereas the second optimization represents the results obtained for Eq. (24b). $\bar{T} = \text{wet-}T_g + 37\,°\text{C}$, therefore, $a_T(\text{wet-}T_g + 37\,°\text{C}) = 1$
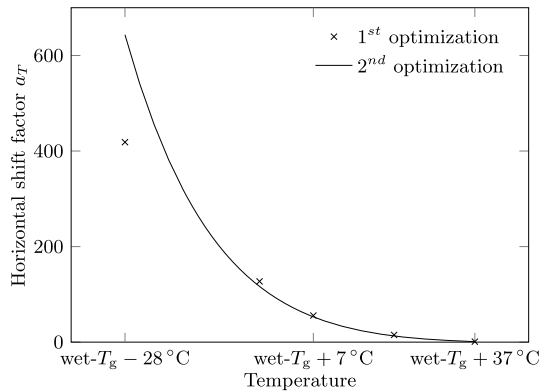
Fig. 11 Evolution of the temperature-dependent vertical shift factor g_0. The first optimization values represent the results obtained without representing g_0 as a function, whereas the second optimization represents the results obtained for Eq. (24c)
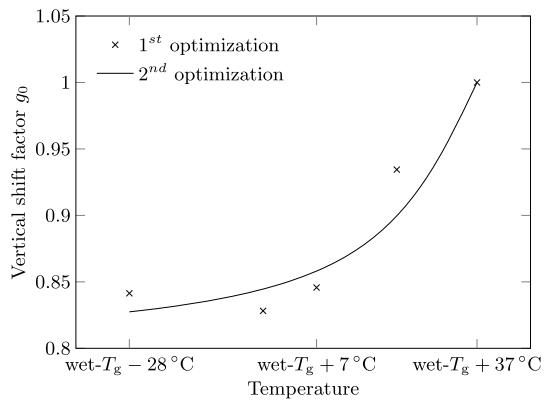
Table 1 Values of the normalized viscoelastic parameters

| n	0	1	2	3	4	5	6	7	8
$\bar{\lambda}_n$ (s^{-1})	–	10^{-6}	10^{-5}	10^{-4}	10^{-3}	10^{-2}	10^{-1}	10^{0}	10^{1}
$\bar{S}_n$	1	31.9191	10.5949	1.0544	0.7931	0.2653	0.1737	0.0470	0.0416

Table 2 Values of the material parameters for μ, a_T, and g_0 obtained after the second optimization

μ_0	μ_1	a_0	a_1	b_0	b_1
0.6825	0.0105	0.4631	0.6316	0.1285	−0.0661

were not fully recovered in some instances. However, the evolution of the strain jump between the end of the creep phase and the beginning of the recovery phase as a function of the ageing time provides a direct and unambiguous means to evaluate if ageing had a global effect on the creep compliance.

Figure 12 plots the normalized strain jump ε_0^r between the creep and recovery phases as a function of the ageing time for various temperatures. The figure shows that little ageing occurred between wet-$T_g - 28\,°$C and wet-wet-$T_g + 7\,°$C, whereas the material exhibited detectable ageing for wet-$T_g + 22\,°$C and wet-$T_g + 37\,°$C.

Fig. 12 Evolution of normalized strain jump ε_0^r between the creep and recovery phases as a function of the ageing time for various temperatures
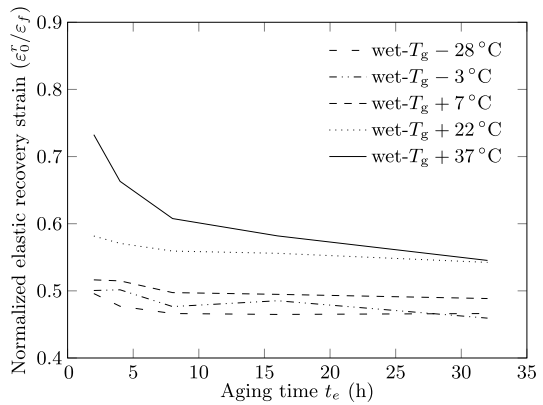
Fig. 13 Normalized predicted creep compliances for various ageing times at (**a**) wet-$T_g - 3$ °C and (**b**) wet-$T_g + 37$ °C. The figure shows that ageing has a more severe affect at higher temperature

(a)

(b)
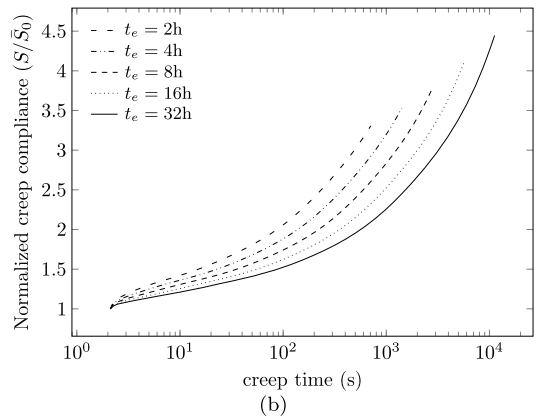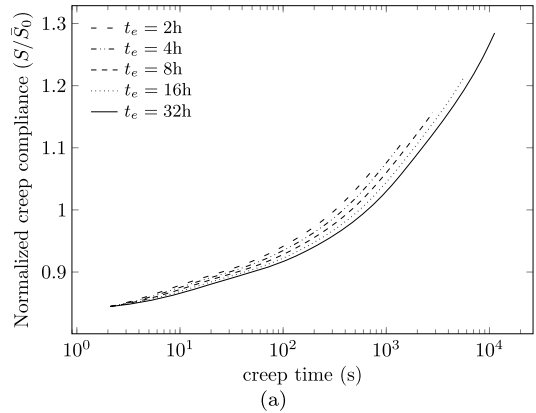
Figure 13 shows the predicted creep compliances for various ageing times at wet-$T_g -$ 3 °C and wet-$T_g + 37$ °C. It can be seen that the model captures the same tendencies as those of Fig. 12 since for a fixed creep time, the creep compliance at wet-$T_g + 37$ °C exhibits a much more important decrease as a function of the ageing time than that at wet-$T_g - 3$ °C.

Fig. 14 Complex thermo-mechanical histories used to validate the model. The material was submitted to series of temperature up- and -down-jumps and creep tests for $\sigma_0 = 0.5\sigma_{max}$. Temperatures T_1, T_2, T_3, and T_4 correspond to wet-$T_g - 28$ °C, wet-$T_g - 3$ °C, wet-$T_g + 22$ °C, and wet-$T_g + 37$ °C, respectively
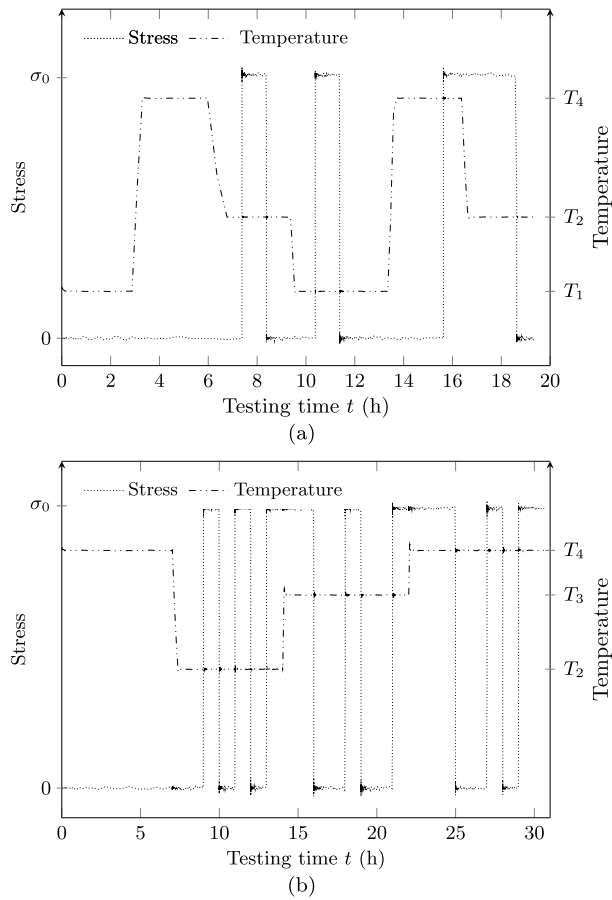

4.4 Validation of the model with a complex thermo-mechanical history

The model proposed previously was validated by submitting the material to complex thermo-mechanical histories and comparing the experimental data to the model predictions. The material was submitted to series of temperature up- and down-jumps and three-point bending creep tests (see Fig. 14). As for the isothermal tests, initial tests with only the thermal histories and a constant load were performed. The results of these tests were subtracted to the results of the tests with the loading histories.

Figure 14 shows the two complex thermo-mechanical histories imposed on the samples, whereas Fig. 15 reports the experimental and predicted strains. The predicted strains were represented for four different models: (i) a simple viscoelastic model, (ii) a viscoelastic model including temperature effects, (iii) a viscoelastic model including ageing effects, (iv) a viscoelastic model including temperature and physical ageing effects. Figure 15 shows that the model including temperature and physical ageing effects predicts the experimental data best for the two independent thermo-mechanical load histories. In particular, the model predicts two behaviors related to temperature changes in Fig. 15a: (i) at $t \sim 13.5$ h, the temperature was increased from wet-$T_g - 28$ °C to wet-$T_g + 37$ °C, which led to an increased compliance and full recovery of the remaining strain; (ii) at $t \sim 16$ h, the temperature

Fig. 15 Experimental data and model predictions for the mechanical strains obtained with the complex thermo-mechanical histories presented in Fig. 14. VE model, Model with T, Model with t_e, and Model with T and t_e represents the model predictions with a simple viscoelastic model, a viscoelastic model including temperature effects, a viscoelastic model with physical ageing effects, and a viscoelastic model including temperature and physical ageing effects, respectively. Strains were normalized by the strain at failure obtained from tensile tests on nonaged samples at wet-$T_g - 28$ °C, ε_f
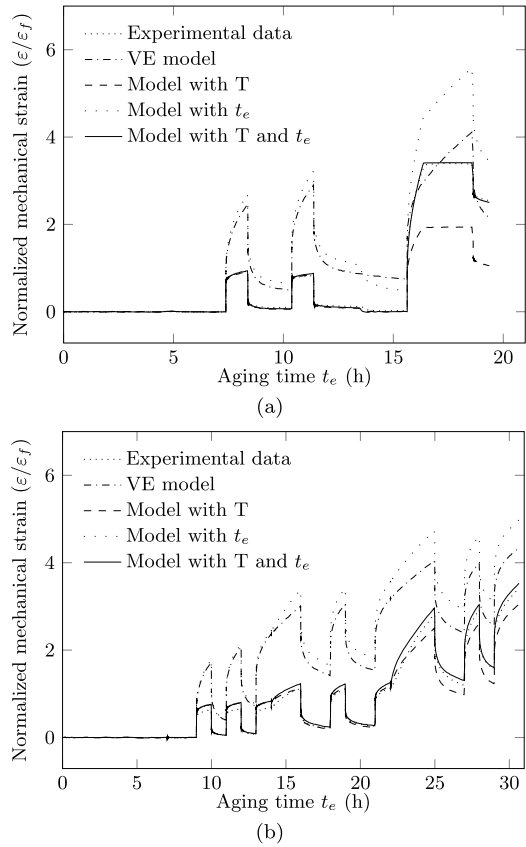
was decreased from wet-$T_g + 37$ °C to wet-$T_g - 3$ °C while the creep stress was maintained. The material became much stiffer, and the creep strain did not increase anymore. Both phenomena are very well predicted by the model. For the second complex thermo-mechanical history of Fig. 15b, the results do not fit the experimental data with as good accuracy as in Fig. 15a for the lower temperatures. However, the overall fit remains very good, and the main features are captured.

5 Conclusions

The main objective of this work was to propose a model for representing the effect of physical ageing on the viscoelastic behavior of MVK-10 polyimide over a wide range of temperatures. The material was submitted to a series of creep and recovery tests at various temperatures. The model proposed is based on the constitutive theories proposed by Schapery. The principal conclusions are as follows:

1. The material was found to be linearly viscoelastic with respect to stress over the range of temperatures, ageing times, and creep stresses studied.
2. The Poisson ratio was found to be independent of time. Therefore, the 3D viscoelastic model could be simplified to a 1D model with a constant Poisson ratio.

3. The model led to an excellent fit of the isothermal creep data at various temperatures. Moreover, the model was validated with complex thermo-mechanical histories. An equivalent ageing time was defined to account for the nonisothermal histories. The predicted data fitted the experimental data very well.

References

Biot, M.A.: Theory of stress–strain relations in anisotropic viscoelasticity and relaxation phenomena. J. Appl. Phys. **25**(11), 1385–1391 (1954)

Bradshaw, R.D., Brinson, L.C.: Physical aging in polymers and polymer composites: An analysis and method for time-aging time superposition. Polym. Eng. Sci. **37**(1), 31–44 (1997a)

Bradshaw, R.D., Brinson, L.C.: Recovering nonisothermal physical aging shift factors via continuous test data: Theory and experimental results. J. Eng. Mater. Technol. **119**, 233–241 (1997b)

Bradshaw, R.D., Brinson, L.C.: A continuous test data method to determine a reference curve and shift rate for isothermal physical aging. Polym. Eng. Sci. **39**(2), 211–235 (1999)

Caruthers, J.M., Adolf, D.B., Chambers, R.S., Shrikhande, P.: A thermodynamically consistent, nonlinear viscoelastic approach for modeling glassy polymers. Polymer **45**(13), 4577–4597 (2004)

Crochon, T., Schönherr, T., Li, C., Lévesque, M.: On finite-element implementation strategies of Schapery-type constitutive theories. Mech. Time-Depend. Mater. **14**, 359–387 (2010)

Drozdov, A.D.: A constitutive model in finite viscoelasticity with an entropy-driven material clock. Math. Comput. Model. **25**(11), 45–66 (1997)

Guo, Y., Bradshaw, R.D.: Isothermal physical aging characterization of polyether–ether–ketone (PEEK) and Polyphenylene sulfide (PPS) films by creep and stress relaxation. Mech. Time-Depend. Mater. **11**(1), 61–89 (2007)

Guo, Y., Bradshaw, R.D.: Long-term creep of polyphenylene sulfide (PPS) subjected to complex thermal histories: The effects of nonisothermal physical aging. Polymer **50**(16), 4048–4055 (2009)

Guo, Y., Wang, N., Bradshaw, R.D., Brinson, L.C.: Modeling mechanical aging shift factors in glassy polymers during nonisothermal physical aging. I. Experiments and KAHR-a_{te} model prediction. J. Polym. Sci., Part B, Polym. Phys. **47**(3), 340–352 (2009)

Haj-Ali, R.M., Muliana, A.H.: Numerical finite element formulation of the Schapery non-linear viscoelastic material model. Int. J. Numer. Methods Eng. **59**, 25–45 (2004)

Jones, D.C.: Nanomechanical Characterization of High Temperature Polymer Matrix Composite Resin: PMR-15 Polyimide. Ph.D. Thesis, University of Kentucky Master's Theses (2009)

Knauss, W.G., Emri, I.: Non-linear viscoelasticity based on free volume consideration. Comput. Struct. **13**(1–3), 123–128 (1981)

Knauss, W.G., Emri, I.: Volume change and the nonlinearly thermo-viscoelastic constitution of polymers. Polym. Eng. Sci. **27**(1), 86–100 (1987)

Kovacs, A.J.: Transition vitreuse dans les polymères amorphes. Etude phénoménologique. Fortschr. Hochpolym.-Forsch. **3**, 394–507 (1963)

Kovacs, A.J., Aklonis, J.J., Hutchinson, J.M., Ramos, A.R.: Isobaric volume and enthalpy recovery of glasses. II. A transparent multiparameter theory. J. Polym. Sci., Part B, Polym. Phys. **17**(7), 1097–1277 (1979)

Lai, J., Bakker, A.: 3-D Schapery representation for non-linear viscoelasticity and finite element implementation. Comput. Mech. **18**, 182–191 (1996)

Lévesque, M., Derrien, K., Baptiste, D., Gilchrist, M.D.: On the development and parameter identification of Schapery-type constitutive theories. Mech. Time-Depend. Mater. **12**, 95–127 (2008)

Li, F., Huang, L., Shi, Y., Jin, X., Wu, Z., Shen, Z., Chuang, K.C., Lyon, R.E., Harris, F.W., Cheng, Z.D.: Thermal degradation mechanism and thermal mechanical properties of two high-performance aromatic polyimide fibers. J. Macromol. Sci. B, Phys. **38**(1–2), 107–122 (1999)

Luo, W.: Application of time-temperature-stress superposition principle to nonlinear creep of poly(methyl methacrylate). Key Eng. Mater. **340**, 1091–1096 (2007)

Marais, C., Villoutreix, G.: Analysis and modeling of the creep behavior of the thermostable PMR-15 polyimide. J. Appl. Polym. Sci. **69**(10), 1983–1991 (1998)

Muliana, A.H., Sawant, S.: Responses of viscoelastic polymer composites with temperature and time dependent constituents. Acta Mech. Sin. **204**, 155–173 (2009)

Ohashi, F., Hiroe, T., Fujiwara, K.: Strain-rate and temperature effects on the deformation of polypropylene and its simulation under monotonic compression and bending. Polym. Eng. Sci. **42**(5), 1046–1055 (2002)

Olasz, L., Gudmundson, P.: Viscoelastic model of cross-linked polyethylene including effects of temperature and crystallinity. Mech. Time-Depend. Mater. **9**(4), 23–44 (2005)

Ruggles-Wrenn, M.B., Broeckert, J.L.: Effects of prior aging at 2888C in air and in argon environments on creep response of PMR-15 neat resin. J. Appl. Polym. Sci. **111**, 228–236 (2009)

Sawant, S., Muliana, A.H.: A thermo-mechanical viscoelastic analysis of orthotropic materials. Compos. Struct. **83**, 61–72 (2008)

Schapery, R.A.: Application of thermodynamics to thermomechanical, fracture, and birefringent phenomena in viscoelastic media. J. Appl. Phys. **35**(5), 1451–1465 (1964)

Schapery, R.A.: A theory of nonlinear thermoviscoelasticity based on irreversible thermodynamics. In: Proceedings of the 5th US National Congress on Applied Mechanics. ASME, vol. 511, pp. 1–20 (1966a)

Schapery, R.A.: An engineering theory of nonlinear viscoelasticity with applications. Int. J. Solids Struct. **2**, 407–425 (1966b)

Schapery, R.A.: Nonlinear viscoelastic and viscoplastic constitutive equations based on thermodynamics. Mech. Time-Depend. Mater. **1**, 209–240 (1997)

Struik, L.C.E.: Physical Aging in Amorphous Polymer and Other Materials. Elsevier, Amsterdam (1978)

Struik, L.C.E.: Dependence of relaxation times of glassy polymers on their specific volume. Polymer **29**(8), 1347–1353 (1988)

Sullivan, J.L., Blais, E.J., Houstan, D.: Physical aging in the creep behavior of thermosetting and thermoplastic composites. Compos. Sci. Technol. **47**, 389–403 (1993)

Williams, M.L., Landel, R.F., Ferry, J.D.: The temperature dependence of relaxation mechanisms in amorphous polymers and other glass-forming liquids. J. Am. Chem. Soc. **77**(14), 3701–3707 (1955)

Xiao, X.R., Hiel, C.C., Cardon, A.H.: Characterization and modeling of nonlinear viscoelastic response of PEEK resin and PEEK composites. Compos. Eng. **4**(7), 681–702 (1994)

Zhao, R.: Application of time-ageing time and time-temperature-stress equivalence to nonlinear creep of polymeric materials. Mater. Sci. Forum **575**, 1151–1156 (2008)